Methods of Estimating AC Losses in Superconducting MgB_2 Armature Windings With Spatial and Time Harmonics

Thanatheepan Balachandran, *Member, IEEE*, Noah J. Salk, *Member, IEEE*, Dongsu Lee, *Associate Member, IEEE*, M. D. Sumption, and Kiruba S. Haran, *Fellow, IEEE*

***Abstract*—Recent developments in low ac loss MgB_2 conductors are of significant importance given renewed interest in fully superconducting (SC) machines. Evaluating ac losses in fully SC machines is a critical step in developing feasible designs. In fully SC machines, SC armature windings experience non-uniform rotating magnetic fields, with spatial and temporal harmonics, which has an undisputed impact on ac losses. Existing ac loss models in the literature, which have been validated for stationary sinusoidal external fields, were extended to constant amplitude rotating fields. There is not enough research on validating the ac loss models for rotating non-uniform magnetic fields with harmonics. This paper proposes simplified methods to estimate the ac losses in conductors with non-uniform rotational applied magnetic fields experienced by the armature in a machine's environment. Extended analytical models are proposed to estimate the ac loss in single and multi-filament MgB_2 conductors. The models are then compared against finite element analysis (FEA) results with Power Law loss estimation to evaluate model fidelity.**

***Index Terms*—Ac loss, analytical models, finite element analysis, harmonics, power law, superconducting machines.**

I. Introduction

FULLY superconducting (SC) machines have the potential to achieve the high-power densities [1] required for direct drive wind turbine [2]–[6] and commercial electric aircraft propulsion [7]–[10]. In a fully SC generator, the armature coils will carry time-varying current while being exposed to a rotating magnetic field with some phase delay [11], [12]. These conditions will generate thermal losses within the SC armature coils, a phenomenon known as *ac losses*. Ac losses in the armature windings are the paramount challenge which must be overcome to make SC machines practical. These heat losses must be removed from the armature windings at cryogenic temperatures to keep the superconductors below their critical temperature at an applied field while carrying transport current. The increase in cryogenic loading adversely impacts the power density and efficiency of the machine. Therefore, ac loss is the most important design parameter considered in the design of a fully SC machine. Fully SC machines designers use analytical models to estimate ac losses in their machines and optimize the machine parameters for minimal losses [5], [13]. The loss estimation is performed using the actual field pattern in the armature winding of a superconducting machine obtained from a detailed transient simulation. The resultant field is evaluated in multiple locations of the armature cross-section as shown in Fig. 1. Here, the armature is separated into three radial sections and losses are evaluated in each section. The single point marked represents the field experienced by a single conductor located at that location. The losses in each conductor are estimated using the field observed at that location and then integrated over the volume of the armature winding to evaluate the total loss value.

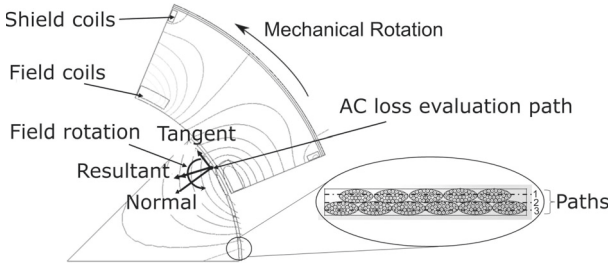

Fig. 1. Cross-section of a fully SC machine.

The armature windings in fully SC machines experience a non-uniform rotating magnetic fields with spatial and temporal harmonics which impact the ac losses. Various analytical ac loss models for the case of a stationary and sinusoidal applied magnetic field have been proposed and experimentally validated in the literature [14]–[16]. These models were extended to evaluate the case of a constant amplitude rotating applied magnetic field [12], [14], [17], [19]–[20]. Ac losses are impacted by the harmonics present in the applied field as well as in the transport current. Several works have focused on capturing the impact of harmonics in the transport current on ac losses [21]–[24].

Manuscript received November 30, 2021; revised April 9, 2022; accepted May 20, 2022. Date of publication June 15, 2022; date of current version June 30, 2022. This work was supported in part by NASA's University Leadership Initiative (ULI) Award on Center for High-Efficiency Electrical Technologies for Aircraft (CHEETA) under Grant 80NSSC19M0125, and in part by NSF under Award 1807823.

Thanatheepan Balachandran and Kiruba S. Haran are with the Department of Electrical and Computer Engineering, University of Illinois Urbana-Champaign, Urbana, IL 61801 USA.

Noah J. Salk and Dongsu Lee are with the Hinetics LLC, Champaign, IL 61820 USA.

M. D. Sumption is with the Department of Material Science and Engineering, The Ohio State University, Columbus, OH 43210 USA.

Color versions of one or more figures in this article are available at https://doi.org/10.1109/TASC.2022.3181535.

Digital Object Identifier 10.1109/TASC.2022.3181535

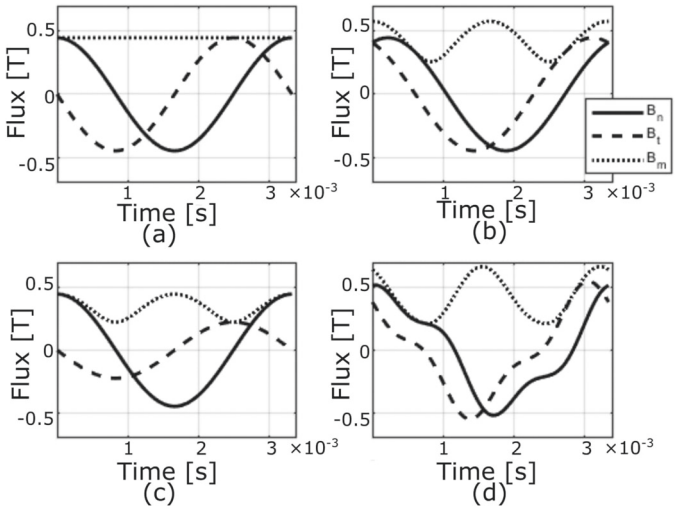

Fig. 2. Applied tangential and normal field amplitude waveforms with the resultant field magnitude. (a) Constant rotating field. (b) Non-uniform rotational field created by a phase angle difference. (c) Non-uniform rotational field created by an amplitude difference. (d) Non-uniform rotational field created by superposition of harmonics.

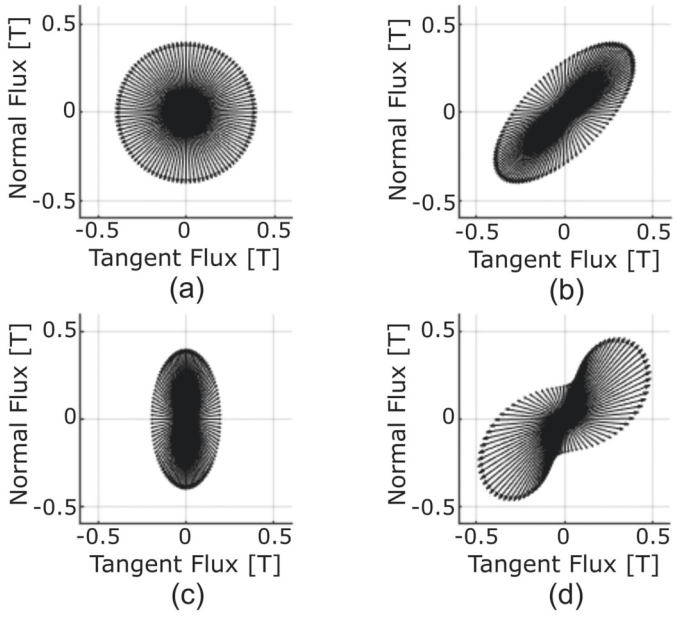

Fig. 3. Vector plot of a rotational field experienced by an armature conductor. (a) Constant rotating field. (b) Non-uniform rotational field created by a phase angle difference. (c) Non-uniform rotational field created by an amplitude difference. (d) Non-uniform rotational field created by superposition of harmonics.

Capturing the additional loss due to a sinusoidal transverse magnetic field with ac ripples has been attempted by various researchers [25]–[27] but remains a challenge for a non-uniform rotating magnetic field. A comparison between the constant rotating field and non-uniform rotating field experienced by a single conductor in an actively shielded fully SC machine is shown in Figs. 2 and 3. This shows how the spatial harmonics influence the field experienced by the armature conductors. Available analytical methods do not capture these effects on ac losses and therefore necessitate extended models to include losses associated with non-uniform rotating fields. Analytical models derived for this special scenario are modified from stationary field models with various assumptions [28]. There are several ongoing efforts to measure losses in HTS tapes experiencing rotating magnetic fields, but loss prediction models have yet to be validated for MgB_2 conductors [12], [29], [30].

This paper proposes simplified methods to estimate ac losses in superconductors with simulated current and field wave forms experienced by an armature conductor in a machine environment. Proposed analytical models are extended from available models in the literature to capture non-uniform rotational magnetic field with superposition of harmonics. Spatial and temporal harmonics obtained from a transient fully SC machine analysis are fed into the analytical model to estimate the losses. These results are then compared against finite element analysis (FEA) results to evaluate model fidelity. The analytical models are then refined to capture different parameters influencing ac losses in machine application. A 2D model of a single and multi-filamentary conductor is used to capture hysteresis, coupling and eddy current losses. The Power Law method is used to model the SC filaments while metallic matrix and sheath materials are modeled with isotropic resistivities. The presence of magnetic sheath materials in the conductor also affect the ac losses and are analyzed by various researchers [31]–[35]. This paper assumes a non-magnetic sheath material in the conductor. The temperature dependence of the parameters is neglected with the assumption that the machine will be maintained at 20 K.

II. Methods to Evaluate AC Loss With Harmonics

Various analytical models have been proposed in the literature to evaluate ac losses in multi-filamentary MgB_2 superconductors [36]–[39]. These approaches use conductor geometric properties and the applied field and current characteristics to estimate losses per unit volume. Carr proposed an extension to models for stationary fields to estimate losses in constant amplitude rotating fields [14]. These models are used in [40]–[42] to estimate losses. Wilson [15] proposed an analytical model to estimate losses in multi-filamentary conductors. This approach uses a loss function $\Gamma(\beta)$ to capture the dependence of hysteresis loss on the applied field strength. These models were used to estimate losses in several applications [43], [44]. Hysteresis and coupling losses are the dominant ac loss factors in armature windings. To accommodate the influence of non-uniform rotating fields, two methods are proposed: the superposition of harmonic losses and the integration of instantaneous losses. The superposition of harmonics method evaluates the total losses by adding the individual losses contributed by each harmonic, similar to how iron losses are often calculated [45]. Using a Fourier transform, any applied transverse field to a conductor can be written as the summation of two spatially orthogonal alternating sinusoidal fields with a 90° phase difference:

$$\vec{B} = \vec{x}\sum_{i}^{n} B_{xi,m}\sin(\omega_i t) + \vec{y}\sum_{i}^{n} B_{yi,m}\cos(\omega_i t) \quad (1)$$

$$\omega_i = \omega_f i = 2\pi f i \quad (2)$$

TABLE I
MgB_2 CONDUCTOR DATASUPPLIER: HYPER TECH RESEARCH

Parameter	Symbol	Multi filament	Single filament
SC outer diameter [mm]	D_0	0.32	0.32
Filament diameter [mm]	d_f	0.01	0.124
Number of filaments	n_f	114	1
SC fill factor	λ	0.15	0.15
Effective transverse resistivity [Ω-mm]	ρ_{eff}	1.25E-4	3.65E-4
Twist pitch [mm]	L_p	5	-

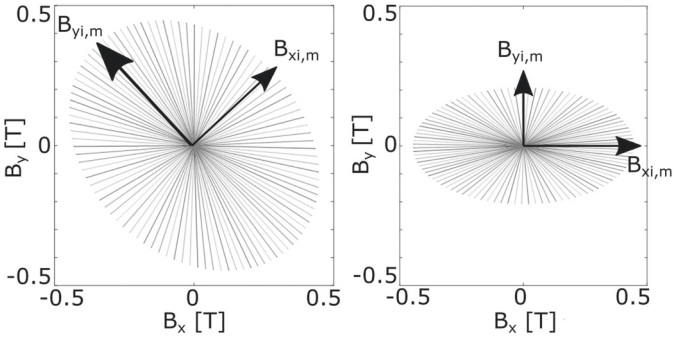

Fig. 4. Major and minor axis peak field magnitude evaluated for two scenarios.

where, $\vec{x}$ and $\vec{y}$ represent the two orthogonal axes considered, f is the fundamental frequency, ω_f if the fundamental angular velocity, i is the order of harmonic, $B_{xi,m}$ is the i^{th} harmonic field amplitude chosen in the $\vec{x}$ direction, $B_{yi,m}$ is the i^{th} harmonic field amplitude chosen in the $\vec{y}$ direction, and t is the time. To find the hysteresis losses generated by each harmonic, losses are multiplied by a factor of R. This is computed in a similar manner to the uniform rotating-field models in [14] by comparing the resultant harmonic vector waveform to the fundamental pure sinusoidal waveform. Evaluation of the resultant R factor is as follows:

$$|\dot{\vec{B}}_i| = |\vec{x} i\omega_f B_{xi,m}\cos(i\omega_f t) - \vec{y} i\omega_f B_{yi,m}\sin(i\omega_f t)| \quad (3)$$

$$R_i = \frac{\int_0^{\frac{2\pi}{\omega}} |\dot{\vec{B}}_i| dt}{\int_0^{\frac{2\pi}{\omega}} |\omega_f B_{m,i}\cos(\omega_f t)| dt} \quad (4)$$

where $\dot{\vec{B}}_i$ is the time derivative of the i^{th} harmonic applied field and $B_{m,i}$ corresponds to the peak magnitude of the resultant rotating field. Once the R factor is found, hysteresis losses can be evaluated as follows:

$$P_h = \sum_{i=1}^{N} R_i \frac{8}{3\pi} B_{m,i} J_{c,i}(B_{m,i}) f_i \lambda d_f \quad (5)$$

where N is the total number of harmonics, $J_{c,i}(B_{m,i})$ is the critical current density corresponding to the i^{th} harmonic peak field, and both d_f and λ are conductor properties tabulated in Table I. Eddy current and coupling losses are also calculated for individual harmonics and added together. Since there is a phase difference between the tangential and normal components, major and minor axis peaks of the resultant waveform are used to estimate the losses as shown in Fig. 4. The total loss can be evaluated as:

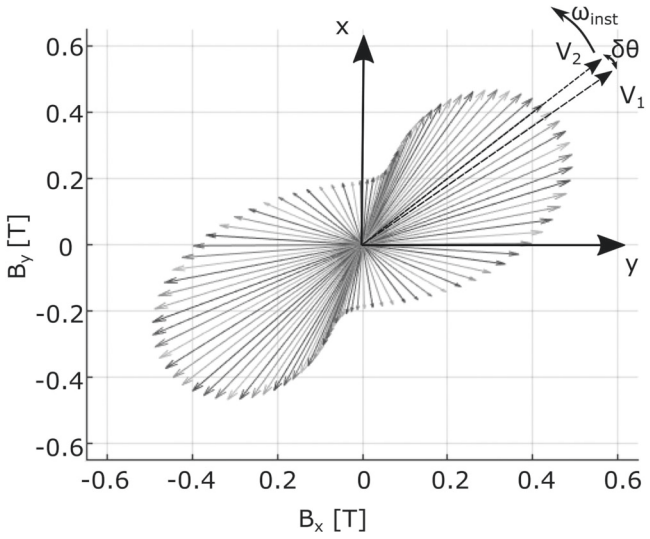

Fig. 5. Rotating non-uniform magnetic field.

$$P_{ei} = \frac{D_0^2}{4k\rho_{eff}} \sum_{i=1}^{N} \left((B_{xi,m} f_i)^2 + (B_{yi,m} f_i)^2\right) \quad (6)$$

$$P_{ci} = \frac{L_p^2}{n\rho_{eff}} \sum_{i=1}^{N} \left((B_{xi,m} f_i)^2 + (B_{yi,m} f_i)^2\right) \quad (7)$$

where $k = 4$ and $n = 2$ are constants determined for a circular conductors, D_0 and L_p are conductor properties tabulated in Table I.

The instantaneous loss method evaluates the energy loss at each instant and integrates over a period to calculate the average power loss. For a circular SC wire with diameter D_0 and external applied transverse field B, the cyclic hysteresis loss P_h can be written as:

$$\frac{P}{V} = \int_0^T \frac{2J_c}{3\pi} D_0 |\dot{B}| dt \quad (8)$$

where, $|\dot{B}|$ is the absolute value of the time derivative of the applied field, J_c is the critical current density at peak, B, and T is the period. For a rotating, non-uniform magnetic field, an additional angle derivative of the rotating field, $B\frac{d\theta}{dt}$, was added to capture the rotating field effects.

$$\dot{B} = \left(\frac{dB}{dt} + B\frac{d\theta}{dt}\right) \quad (9)$$

where θ indicates the rotational direction. Instantaneous losses are evaluated from FEA results based on the rotational field experienced by a conductor in the armature. Field data can be given in the normal and tangential referenced coordinate system or in any random orthogonal coordinate system as shown in Fig. 5. Two consecutive resultant vector fields V_1 and V_2 are denoted as follows:

$$V_1 = [B_{x1}, B_{y1}, 0], V_2 = [B_{x2}, B_{y2}, 0] \quad (10)$$

then, the angle between the two consecutive field vectors is evaluated as:

$$\delta\theta = \cos^{-1}\left(\frac{V_1.V_2}{|V_1|.|V_2|}\right) \tag{11}$$

and the instantaneous loss is evaluated as:

$$P_{h,inst} = \frac{4J_c\lambda}{3\pi}\left(\frac{dB}{dt} + B\frac{d\theta}{dt}\right) \tag{12}$$

By integrating over one cycle, the cyclic energy loss is evaluated as:

$$E_{h,cyclic} = \sum P_{h,inst}\Delta t \tag{13}$$

Multiplying that energy loss by the average frequency gives an average hysteretic ac loss for the SC wire:

$$P_h = \frac{1}{T}E_{h,cyclic} \tag{14}$$

where T is the period. Similarly, eddy current loss can be evaluated as:

$$P_{e,inst} = \frac{1}{16\rho_{eff}}\left(\frac{dB}{dt} + B\frac{d\theta}{dt}\right)^2 D_o^2 \tag{15}$$

$$E_{e,cyclic} = \sum P_{e,inst}\Delta t \tag{16}$$

$$P_e = \frac{1}{T}E_{e,cyclic} \tag{17}$$

and coupling current loss can be evaluated as:

$$P_{c,inst} = \frac{L_p^2}{8\pi^2\rho_{eff}}\left(\frac{dB}{dt} + B\frac{d\theta}{dt}\right)^2 \tag{18}$$

$$E_{c,cyclic} = \sum P_{c,inst}\Delta t \tag{19}$$

$$P_c = \frac{1}{T}\sum E_{c,cyclic} \tag{20}$$

III. AC Loss Verification

Several numerical analysis methods utilizing FEA tools have been proposed to evaluate the ac losses in SC cables under sinusoidal external field [46], [47]. Numerical models for MgB_2 conductors in high power transmission cables are presented in [48]. A 12 filament superconductor with 1.1 mm wire outer diameter is modeled and self-field losses are evaluated. In this paper the Power Law is used to compute the spatial receptivity of the superconductor and subsequent losses within the finite element method. A fourth-order polynomial fit is used to extrapolate J_c vs. B data for an example conductor provided by HyperTech Research, and Kim-Anderson constants are used in calculating the electric field:

$$J_c(B) = a_4B^4 + a_3B^3 + a_2B^2 + a_1B + a_0 \tag{21}$$

$$n = \frac{n_0}{1 + \frac{B}{B_1}} \tag{22}$$

$$E = E_c\left(\frac{J}{J_c}\right)^{\frac{1}{n}} \tag{23}$$

TABLE II
2.5 MW CHEETA Machine Field Harmonics

n	f[Hz]	Normal B_m [T]	Normal θ [rad]	Tangent B_m [T]	Tangent θ [rad]
1	300	0.418	-23.52	0.209	24.5
3	900	0.107	11.98	0.106	101.96
5	1500	0.017	-99.47	0.017	-9.4
7	2100	0.023	-31.47	0.023	58.3

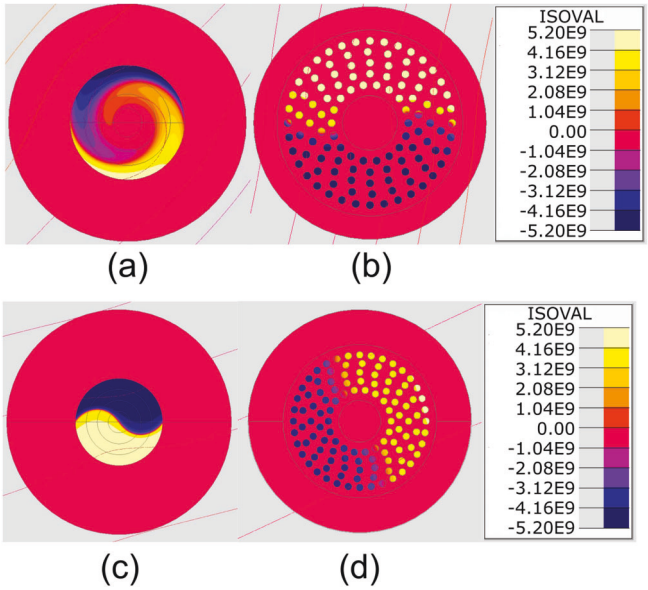

Fig. 6. Current density in single conductor under non-uniform rotating field at 10 Hz. (a) Single filament partial penetration. (b) Multi filament partial penetration. (c) Single filament full penetration. (d) Multi filament full penetration.

$$\rho(J) = \frac{E_c^{(\frac{1}{n})}}{J_c(B)}\left|\frac{J}{J_c(B)}\right|^{(n-1)} \tag{24}$$

$$P_T = \iiint_V (E \cdot J)dV \tag{25}$$

where B is the applied magnetic field, J is the current density, E is the electric field, and constants $a_0 - a_4, n_0, B_1, J_c$ and E_c are unique to the specific conductor chosen and are evaluated from conductor experimental data. A 2D FEA simulation was used to evaluate the losses on a single SC conductor. Losses are evaluated by integrating (25) in the SC filament area and copper area. The MgB_2 conductor is placed in the center of a rotating magnetic field and is surrounded by a copper matrix. Similarly, a multi-filament cable is also placed in the center of the rotating magnetic field.

Specifications of the MgB_2 conductors used in this study are provided in Table I. Air-gap field harmonic data obtained from a transient analysis of the proposed 2.5-MW CHEETA fully SC motor is used to verify the proposed model [13]. Air-gap field harmonic data of this machine is tabulated in Table II. For the initial analysis, single filament and multi-filament conductors are modeled and analyzed in FEA. Fig. 6 shows the current density variation across the conductors at partial and full penetration. The behaviour of a SC element under rotating magnetic fields is quite different from that due to a stationary field. When

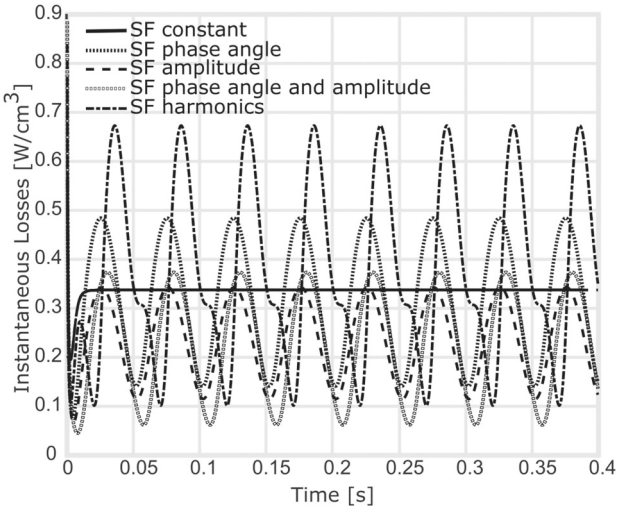

Fig. 7. Instantaneous losses in a single filament conductor in W/cm^3 at 10 Hz.

the field is increased from an initial value of zero, the induced magnetic fields in the SC element are aligned in a direction such to oppose the applied field. However, after one rotation there is a lag between the induced magnetic field and the external applied field, similar to a boundary-edge effect, at the interface between the copper and superconductor. This trend can also be seen in the multi-filamentary conductor as a collective pattern. A 2D flux density distribution across the multi-filamentary conductor is shown in Fig. 6(b) and (d). From the figure, this phenomenon happens at both the bundle level and at the individual filament level based on the local flux density. It can also be seen that the coupling currents dominate in the multi-filament conductors and thus require a detailed 3-D analysis for loss estimation. To simplify the model for comparison, the following scenarios are considered to evaluate the losses on a single filament conductor:

- Scenario 1: Assume a fundamental frequency with a constant rotating field (ideal sinusoidal waveform). Shown in Fig. 3(a).
- Scenario 2: Assume a fundamental frequency with a non-uniform rotating field caused by a phase angle difference. Similar to Fig. 3(b).
- Scenario 3: Assume a fundamental frequency with a non-uniform rotating field caused by an amplitude difference. Similar to Fig. 3(c).
- Scenario 4: Assume a fundamental frequency with a non-uniform rotating field caused by a phase angle and amplitude difference. Similar to Fig. 3(b).
- Scenario 5: Assume a non-uniform field with 1st and 3rd order harmonics with amplitude and phase variation. Similar to 3(d).

These scenarios are also simulated for a multi-filament conductor at 10 Hz. Fig. 7 provides the evaluated instantaneous loss components using FEA modeling. This clearly shows that the constant rotating field has constant losses and all other scenarios create cyclic losses. The instantaneous loss variation shows a close relationship to the applied non-uniform rotating field thus providing support for the ratio constant, R. Fig. 8

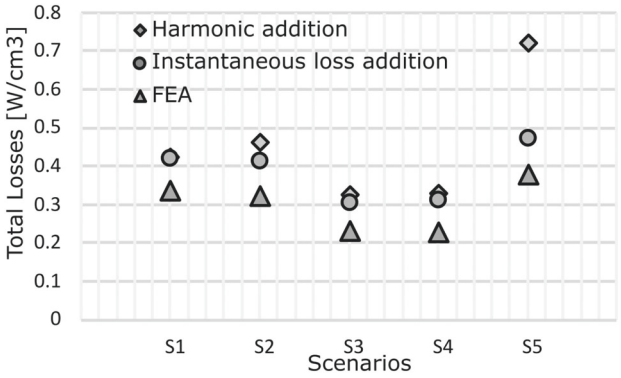

Fig. 8. Average total losses in a single filament conductor in W/cm^3 at 10 Hz.

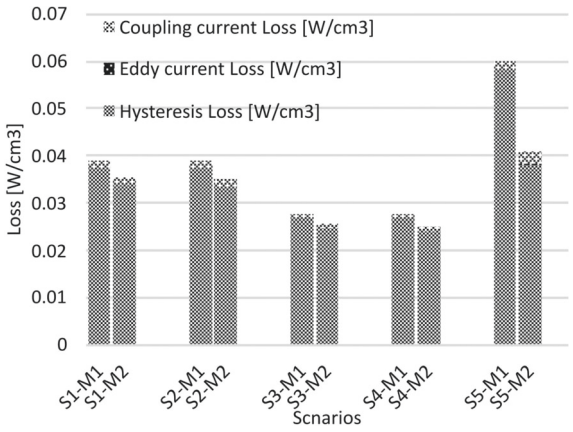

Fig. 9. Average ac loss components in a multi filament conductor in W/cm^3 at 10 Hz.

depicts the evaluated average loss components using analytical models compared to those from FEA. The results show that for single-filament cases, hysteresis and eddy current losses closely align for both of the analytical approaches until harmonics are introduced. When the harmonics are introduced, instantaneous loss evaluation closely matches the FEA simulation. The same analytical models are extended to evaluate the losses in a multi-filament conductor. Fig. 9 shows the average cyclic losses estimated using both of the proposed methods. We can see a similar trend to that of the single conductor case, where the instantaneous loss estimation method shows moderate increments compared to the superposition of harmonics method. Due to the significant coupling currents, a 3D FEA model is necessary to evaluate FEA ac losses in multi-filament conductor and will be explored in future work.

IV. Conclusion and Future Works

AC losses under non-uniform rotating fields are evaluated in single filament and multi-filament MgB_2 armature conductors. The introduction of harmonics in the applied field necessitates adjustments to analytical models to capture the additional impact on losses. Simplified analytical models are proposed to include non-uniform rotating field with harmonics. FEA models are

used to validate the extended analytical methods and estimate losses under an applied non-uniform rotational magnetic field. In the future, 2D winding packs and 3D FEA analysis results for the MgB_2 conductor will be analyzed to further validate the proposed computations.

REFERENCES

[1] K. S. Haran *et al.*, "High power density superconducting rotating machinesdevelopment status and technology roadmap," *Supercond. Sci. Technol.*, vol. 30, no. 12, Nov. 2017, Art. no. 123002. [Online]. Available: https://doi.org/10.1088%2F1361-6668%2Faa833e

[2] S. S. Kalsi, "Superconducting wind turbine generator employing MgB_2 windings both on rotor and stator," *IEEE Trans. Appl. Supercond.*, vol. 24, no. 1, Feb. 2014, Art. no. 5201907.

[3] A. B. Abrahamsen *et al.*, "Comparison of levelized cost of energy of superconducting direct drive generators for a 10-MW offshore wind turbine," *IEEE Trans. Appl. Supercond.*, vol. 28, no. 4, 2018, Art. no. 5208205.

[4] T.-K. Hoang, L. Quéval, C. Berriaud, and L. Vido, "Design of a 20-MW fully superconducting wind turbine generator to minimize the levelized cost of energy," *IEEE Trans. Appl. Supercond.*, vol. 28, no. 4, Jun. 2018, Art. no. 5206705.

[5] F. Lin, R. Qu, D. Li, Y. Cheng, and J. Sun, "Electromagnetic design of 13.2-MW fully superconducting machine," *IEEE Trans. Appl. Supercond.*, vol. 28, no. 3, Apr. 2018, Art. no. 5205905. .

[6] M. Saruwatari *et al.*, "Design study of 15-MW fully superconducting generators for offshore wind turbine," *IEEE Trans. Appl. Supercond.*, vol. 26, no. 4, Jun. 2016, Art. no. 5206805.

[7] C. D. Manolopoulos *et al.*, "Design of superconducting AC propulsion motors for hybrid electric aerospace," in *Proc. AIAA/IEEE Electric Aircr. Technol. Symp. (EATS)*, 2018, pp. 1–9.

[8] A. Patel, V. Climente-Alarcon, A. Baskys, B. A. Glowacki, and T. Reis, "Design considerations for fully superconducting synchronous motors aimed at future electric aircraft," in *Proc. IEEE Int. Conf. Elect. Syst. Aircraft, Railway, Ship Propulsion Road Veh. Int. Transp. Electrific. Conf.*, 2018, pp. 1–6.

[9] Y. Terao, A. Seta, H. Ohsaki, H. Oyori, and N. Morioka, "Lightweight design of fully superconducting motors for electrical aircraft propulsion systems," *IEEE Trans. Appl. Supercond.*, vol. 29, no. 5, Aug. 2019, Art. no. 5202305.

[10] Y. Terao, W. Kong, H. Ohsaki, H. Oyori, and N. Morioka, "Electromagnetic design of superconducting synchronous motors for electric aircraft propulsion," *IEEE Trans. Appl. Supercond.*, vol. 28, no. 4, Jun. 2018, Art. no. 5208005.

[11] D. Nguyen, P. Sastry, G. Zhang, D. Knoll, and J. Schwartz, "AC loss measurement with a phase difference between current and applied magnetic field," *IEEE Trans. Appl. Supercond.*, vol. 15, no. 2, pp. 2831–2834, Jul. 2005.

[12] R. Schafer and C. Heiden, "Dissipation in cylindrical type-II superconductors rotating in a magnetic field," *IEEE Trans. Magn.*, vol. 13, no. 1, pp. 201–204, Jan. 1977.

[13] T. Balachandran, D. Lee, N. Salk, and K. S. Haran, "A fully superconducting air-core machine for aircraft propulsion," *IOP Conf. Series: Mater. Sci. Eng.*, vol. 756, Jun. 2020, Art. no. 012030. [Online]. Available: https://doi.org/10.1088%2F1757-899x%2F756%2F1%2F012030

[14] J. W. Carr, *AC Loss and Macroscopic Theory of Superconductors*. London, U.K.: CRC Press, 2001.

[15] M. N. Wilson, *Superconducting Magnets*. Oxford, U.K. Clarendon: Oxford, 1983.

[16] M. Ashkin, "Flux distribution and hysteresis loss in a round superconducting wire for the complete range of flux penetration," *J. Appl. Phys.*, vol. 50, no. 11, pp. 7060–7066, 1979. [Online]. Available: https://doi.org/10.1063/1.325866

[17] C. P. Bean, "Rotational hysteresis loss in high–field superconductors," *J. Appl. Phys.*, vol. 41, no. 6, pp. 2482–2483, 1970. [Online]. Available: https://doi.org/10.1063/1.1659249

[18] C. Pang, A. Campbell, and P. McLaren, "Losses in Nb/Ti multifilamentary composite when exposed to transverse alternating and rotating fields," *IEEE Trans. Magn.*, vol. 17, no. 1, pp. 134–137, Jan. 1981.

[19] J. le G. Gilchrist, "Rotating fields and flux pinning," *J. Phys. D: Appl. Phys.*, vol. 5, no. 12, pp. 2252–2265, Dec. 1972. [Online]. Available: https://doi.org/10.1088/0022-3727/5/12/314

[20] A. Fevrier and J. Renard, "Losses in Nb Ti multifilamentary composites subjected to a rotating magnetic induction," *IEEE Trans. Magn.*, vol. 15, no. 1, pp. 256–259, Jan. 1979.

[21] B. Douine, J. Leveque, and A. Rezzoug, "AC loss measurements of a high critical temperature superconductor transporting sinusoidal or non-sinusoidal current," *IEEE Trans. Appl. Supercond.*, vol. 10, no. 1, pp. 1489–1492, Mar. 2000.

[22] M. Yazdani-Asrami, W. Song, M. Zhang, W. Yuan, and X. Pei, "AC transport loss in superconductors carrying harmonic current with different phase angles for large-scale power components," *IEEE Trans. Appl. Supercond.*, vol. 31, no. 1, Jan. 2021, Art. no. 5900205.

[23] M. Yazdani-Asrami, W. Song, X. Pei, M. Zhang, and W. Yuan, "AC loss characterization of HTS pancake and solenoid coils carrying non-sinusoidal currents," *IEEE Trans. Appl. Supercond.*, vol. 30, no. 5, Aug. 2020, Art. no. 5900709.

[24] W. Song, J. Fang, and Z. Jiang, "Numerical AC loss analysis in HTS stack carrying non-sinusoidal transport current," *IEEE Trans. Appl. Supercond.*, vol. 29, no. 2, Mar. 2019, Art. no. 5900405.

[25] V. Sokolovsky, V. Meerovich, M. Spektor, G. A. Levin, and I. Vajda, "Losses in superconductors under non-sinusoidal currents and magnetic fields," *IEEE Trans. Appl. Supercond.*, vol. 19, no. 3, pp. 3344–3347, Jun. 2009.

[26] M. Yazdani-Asrami, W. Song, M. Zhang, W. Yuan, and X. Pei, "Magnetization loss in HTS coated conductor exposed to harmonic external magnetic fields for superconducting rotating machine applications," *IEEE Access*, vol. 9, pp. 77 930–77 937, 2021.

[27] M. Tsuda, Y. Nakaide, D. Miyagi, and T. Hamajima, "Estimation method of AC losses in HTS tape against a distorted current and/or a distorted magnetic field with harmonic components," *IEEE Trans. Appl. Supercond.*, vol. 25, no. 3, Jun. 2015, Art. no. 6605605.

[28] M. Sumption, "AC loss of superconducting materials for very high density motors and generators of hybrid-electric aircraft," in *Proc. AIAA/IEEE Electric Aircr. Technol. Symp.*, 2018, pp. 1–6.

[29] J. P. Murphy *et al.*, "Experiment setup for calorimetric measurements of losses in HTS coils due to AC current and external magnetic fields," *IEEE Trans. Appl. Supercond.*, vol. 23, no. 3, Jun. 2013, Art. no. 4701505.

[30] P. K. Ghoshal, T. A. Coombs, and A. M. Campbell, "Calorimetric method of AC loss measurement in a rotating magnetic field," *Rev. Sci. Instruments*, vol. 81, no. 7, 2010, Art. no. 074702. [Online]. Available: https://doi.org/10.1063/1.3458003

[31] P. K. c *et al.*, "Magnetic interaction of an iron sheath with a superconductor," *Supercond. Sci. Technol.*, vol. 16, no. 10, pp. 1195–1201, Sep. 2003. [Online]. Available: https://doi.org/10.1088/0953-2048/16/10/312

[32] J. Kováč, J. Šouc, P. Kováč, and I. Hušek, "AC losses of single-core MgB_2 wires with different metallic sheaths," *Physica C: Supercond. Appl.*, vol. 519, pp. 95–99, 2015. [Online]. Available: https://www.sciencedirect.com/science/article/pii/S0921453415002634

[33] M. Majoros, M. D. Sumption, M. A. Susner, M. Tomsic, M. Rindfleisch, and E. W. Collings, "AC losses in MgB_2 multifilamentary strands with magnetic and non-magnetic sheath materials," *IEEE Trans. Appl. Supercond.*, vol. 19, no. 3, pp. 3106–3109, Jun. 2009.

[34] Y. Nikulshin, Y. Yeshurun, and S. Wolfus, "Effect of magnetic sheath on filament AC losses and current distribution in MgB_2 superconducting wires: Numerical analysis," *Supercond. Sci. Technol.*, vol. 32, no. 7, Jun. 2019, Art. no. 075007. [Online]. Available: https://doi.org/10.1088/1361-6668/ab13d9

[35] S. Safran, S. Souc, F. Gomory, P. Kovac, and A. Gencer, "Experimentally determined magnetization AC losses of mono and multifilamentary MgB_2 wires," *J. Supercond. Novel Magnetism*, vol. 26, no. 5, pp. 1557–1561, 2013.

[36] N. Magnusson, A. Abrahamsen, D. Liu, M. Runde, and H. Polinder, "Hysteresis losses in MgB_2 superconductors exposed to combinations of low AC and high DC magnetic fields and transport currents," *Physica C: Supercond. Appl.*, vol. 506, pp. 133–137, 2014. [Online]. Available: https://www.sciencedirect.com/science/article/pii/S0921453414001919

[37] S. Choi, T. Kiyoshi, J. H. Kim, and S. X. Dou, "AC loss in MgB_2 superconducting wires at various operating temperatures," *IEEE Trans. Appl. Supercond.*, vol. 21, no. 3, pp. 3342–3346, Jun. 2011.

[38] K. Kajikawa *et al.*, "Dependence of transport-current losses in MgB_2 superconducting wire on temperature and frequency," *IEEE Trans. Appl. Supercond.*, vol. 20, no. 3, pp. 2111–2114, Jun. 2010.

[39] H. Taxt, N. Magnusson, M. Runde, and S. Brisigotti, "AC loss measurements on multi-filamentary MgB_2 wires with non-magnetic sheath materials," *IEEE Trans. Appl. Supercond.*, vol. 23, no. 3, Jun. 2013, Art. no. 8200204.

[40] M. D. Sumption, "AC loss of superconducting materials- refined loss estimates for very high density motors and generators for hybrid-electric aircraft: MgB_2 wires, coated conductor tapes and wires," in *Proc. AIAA Propulsion Energy Forum,* 2019, Art. no. 4495. [Online]. Available: https://arc.aiaa.org/doi/abs/10.2514/6.2019-4495

[41] Y. Terao, M. Sekino, and H. Ohsaki, "Electromagnetic design of 10 MW class fully superconducting wind turbine generators," *IEEE Trans. Appl. Supercond.*, vol. 22, no. 3, Jun. 2012, Art. no. 5201904.

[42] T. Balachandran, D. Lee, N. Salk, J. Xiao, and K. S. Haran, "Evaluation and mitigation of AC losses in a fully superconducting machine for wind turbine applications," *IEEE Trans. Appl. Supercond.*, vol. 30, no. 4, Jun. 2020, Art. no. 5207005.

[43] D. Kostopoulos, D. Liu, Genani, and H. G. Polinder, "Feasibility study of a 10 MW MgB_2 fully superconducting generator for offshore wind turbines," in *Proc. EWEA Offshore*, 2013, pp. 1–11.

[44] T. Balachandran, D. Lee, and K. S. Haran, "Optimal design of a fully superconducting machine for 10-MW offshore wind turbines," in *Proc. IEEE Int. Electric Machines Drives Conf.*, 2019, pp. 1903–1909.

[45] M. R. Saurabh Kumar Mukerji, M. George, and K. Asaduzzaman, "Eddy currents in solid rectangular cores," *Prog. Electromagn. Res. B*, vol. 7, pp. 117–131, 2008.

[46] C. Lorin and P. J. Masson, "Numerical analysis of the impact of elliptical fields on magnetization losses," *IEEE Trans. Appl. Supercond.*, vol. 23, no. 3, Jun. 2013, Art. no. 8201405.

[47] M. Lyly, V. Lahtinen, A. Stenvall, L. Rostila, and R. Mikkonen, "A time-harmonic approach to numerically model losses in the metal matrix in twisted superconductors in external magnetic field," *IEEE Trans. Appl. Supercond.*, vol. 24, no. 2, Apr. 2014, Art. no. 8200909.

[48] F. Grilli *et al.*, "Numerical modeling of MgB_2 conductors for high power ac transmission," *Physica C: Supercond. Appl.*, vol. 504, pp. 167–171, 2014. [Online]. Available: http://www.sciencedirect.com/science/article/pii/S0921453414001452